14th International Conference on Applications of Statistics and Probability in Civil Engineering, ICASP14
Dublin, Ireland, July 9-13, 2023

Uncertainty quantification and guidance on the use of wind tunnel-informed stochastic wind load models for applications in performance-based wind engineering

Thays G. A. Duarte
Graduate Student, Dept. of Civil and Coastal Engineering, Univ. of Florida, Gainesville, USA

Srinivasan Arunachalam
Graduate Student, Dept. of Civil and Environmental Engineering, Univ. of Michigan, Ann Arbor, USA

Arthriya Subgranon
Assistant Professor, Dept. of Civil and Coastal Engineering, Univ. of Florida, Gainesville, USA

Seymour M. J. Spence
Associate Professor, Dept. of Civil and Environmental Engineering, Univ. of Michigan, Ann Arbor, USA

ABSTRACT: Probabilistic performance-based wind engineering (PBWE) is a state-of-the-art framework that allows for direct uncertainty propagation through the hazard, aerodynamic, structural response, damage, and loss models in assessing the performance of building systems subject to wind loads. To enable the application of PBWE, the aerodynamic model needs to be capable of simulating multi-variate stochastic processes representing the dynamic wind loads acting on the system. For efficient simulation, models based on spectral proper orthogonal decomposition (POD) are of interest because such an approach allows subprocesses to be generated independently while a few spectral modes are needed to adequately represent the fluctuating component of the wind load, hence significantly reducing the computational cost. To ensure that the aerodynamic phenomena observed in the wind tunnel are captured and used to inform the aerodynamic model, a data-driven POD-based stochastic wind model has been recently proposed where wind tunnel data is used to calibrate the spectral modes and eigenvalues of the target load processes. While the proposed model can serve as a general wind simulation tool for any wind direction and geometry, errors associated with such a model need to be quantified and treated properly in applications of PBWE. To investigate the errors, an extensive experimental study on a rectangular building model was conducted at the University of Florida NHERI boundary layer wind tunnel for varying wind directions and experimental settings. In particular, tests were performed for a total duration, at model scale, of 15 minutes and repeated five times in increments of 10 degrees. The datasets were divided into two groups; one was used to define the target spectra while the other was used as a testing set to evaluate the errors. Three types of errors were analyzed including the errors associated with using standard wind tunnel data (e.g., a single 32-second record), numerical scheme, and truncation of spectral modes. Results reveal insights into typical model errors and control techniques that help facilitate the development of practical guidance on the use of the proposed wind tunnel-informed stochastic load model in a PBWE setting.

In Performance-Based Wind Engineering (PBWE) frameworks, one critical step to accurately assess the performance of wind-excited building systems is the simulation of multivariate dynamic wind processes (Chuang and Spence, 2017; Ouyang and Spence, 2020, 2021a,b; Chuang and Spence, 2022; Arunachalam and Spence, 2022). Not only do uncertainties associated with wind processes need to be accounted for, but the aerodynamic phenomena for specific building geometry and wind conditions also need to be adequately modeled. Several stochastic wind models have been developed over the last decades. Among these, spectral representation methods (SRM), and in particular models based on spectral proper orthogonal decomposition (POD), have been widely used in the field of wind engineering due to their computational efficiency and mode truncation capability (Deodatis, 1996; Shinozuka, 1987; Chen and Kareem, 2005; Shinozuka, 1971). Most POD-based stochastic wind models are calibrated from the generalized expression of the covariance or cross-power spectral density (CPSD) matrices of the wind processes. Even though much effort has been placed on defining generalized spectra formulations for estimating along-wind, cross-wind, and torsional responses of systems under wind loads (Kaimal and Finnigan, 1994; Davenport, 1971), there are currently no reliable models that can simulate building-specific aerodynamic effects for general geometry and wind directions.

A data-driven approach has recently been proposed where wind tunnel data is used to calibrate the POD-based stochastic models aimed at reproducing aerodynamic phenomena captured during wind tunnel testing (Suksuwan and Spence, 2018, 2019; Ouyang and Spence, 2020). The significant advantage of the proposed method is its applicability to general building geometry, terrain conditions, and wind directions. However, two main issues arise from using wind tunnel-informed stochastic wind models. First, typical wind tunnel records last from 30 seconds to 1 minute and may not adequately represent the underlying stochastic processes. If these records are used to calibrate the model, errors can propagate to the simulation. Second, the extent of errors associated with using typical wind tunnel records and mode truncation has not yet been investigated.

In order to quantify the errors associated with using the proposed data-driven stochastic wind model, experimental data have been collected on a rectangular model for multiple wind directions (e.g., 0°, 90°). The large set of collected data is divided into two groups: the first is used to define the target spectra, which is later considered as a reference value for error measurement, while the rest is divided into individual 32-second records to estimate errors associated with wind tunnel record variability. To simulate multivariate stationary Gaussian wind loads (i.e., wind forces), the POD-based SRM is employed, and the target spectra are used to calibrate the model. Three error measurements are investigated in this study: errors associated with the variability of wind tunnel records, errors associated with the numerical model, and errors associated with the truncation of modes, with an aim to provide clearer guidance on using this type of approach for simulation of multivariate stationary Gaussian processes.

1. POD-BASED DECOMPOSITION OF THE CPSD

The CPSD matrix of a multivariate stationary random process can be decomposed using the POD method. In particular, the vector-valued stochastic process, $\boldsymbol{F}(t;\alpha) = \{F_1(t;\alpha),...,F_N(t;\alpha)\}^T$, can be expressed in the frequency-domain after a fast Fourier transformation (FFT) in terms of its orthogonal modes, $\boldsymbol{\Phi}(\omega;\alpha)$, as:

$$\boldsymbol{F}(\omega;\alpha) = \sum_{n=1}^{N} \boldsymbol{\Phi}(\omega;\alpha) a_n(\omega;\alpha) \qquad (1)$$

where ω is the frequency, α is the wind direction, N is the number of subproccesses, $\boldsymbol{\Phi}(\omega;\alpha) = [\boldsymbol{\Phi}_1(\omega;\alpha),...,\boldsymbol{\Phi}_N(\omega;\alpha)]$, and $a_n(\omega;\alpha)$ is a component of $\boldsymbol{a}(\omega;\alpha)$, which is the FFT of the expansion series $\boldsymbol{a}(t;\alpha)$. The orthogonal modes are defined as the solution to the following eigenproblem:

$$\boldsymbol{S}_F(\omega;\alpha)\boldsymbol{\Phi}_n(\omega;\alpha) = \Lambda_n(\omega;\alpha)\boldsymbol{\Phi}_n(\omega;\alpha) \qquad (2)$$

where $\boldsymbol{S}_F(\omega;\alpha)$ is the two-sided CPSD matrix of $\boldsymbol{F}(t;\alpha)$, and can also be expressed

in terms of mode functions as $\boldsymbol{S}_F(\omega;\alpha) = \sum_{n=1}^{N} \Lambda_n(\omega;\alpha)\boldsymbol{\Phi}_n(\omega;\alpha)\boldsymbol{\Phi}_n^*(\omega;\alpha)$, where the asterisk represents the conjugate transpose of the eigenvalue matrix, and $\Lambda_n(\omega;\alpha)$ is the corresponding eigenvalue. Through this expression, it can be seen that $\boldsymbol{S}_F(\omega;\alpha)$ can be obtained by summing the contribution of each mode (Chen and Kareem, 2005). The first few modes usually capture most energy, hence allowing the truncation of higher frequency modes with no significant effects on the statistical properties and frequency content of the process.

2. Simulation of Wind Load Process

To simulate the valued-vector stationary Gaussian process, the data-driven spectral POD approach is adopted in this study (Suksuwan and Spence, 2018; Ouyang and Spence, 2020). The data-informed approach uses the CPSD matrix of the wind load process obtained directly from a wind tunnel realization to calibrate the second-order statistics of the stochastic model. Through this approach, each subprocess can be simulated independently using the following mathematical expression:

$$\tilde{\mathbf{F}}_n(t;\alpha) = \sum_{j=0}^{N_\omega - 1} 2|\boldsymbol{\Phi}_n(\omega_j;\alpha)|\sqrt{\Lambda_n(\omega_j;\alpha)\Delta\omega}\times \cos(\omega_j t + \theta_j(\omega_j) + \phi_{nj}) \tag{3}$$

where $\boldsymbol{\Phi}_n(\omega;\alpha)$ and $\Lambda_n(\omega;\alpha)$ are obtained directly from the wind tunnel realization, N_ω is the total number of frequency increments (limited by the Nyquist cut-off frequency), α is the wind direction of the wind tunnel realization, $\Delta\omega$ is the frequency increment with $\omega_j = j\Delta\omega$, ϕ_{nj} is a random number generated from a uniform distribution between $[0, 2\pi]$, and $\theta_j(\omega_j)$ is the phase angle such that $\theta_j(\omega_j) = \tan^{-1}\left(\mathrm{Im}(\boldsymbol{\Phi}_n(\omega_j;\alpha))/\mathrm{Re}(\boldsymbol{\Phi}_n(\omega_j;\alpha))\right)$. The summation of the first N_m ($N_m < N$) subprocesses, $\tilde{\mathbf{F}}_n(t;\alpha)$, associated with the largest eigenvalues gives the reduced-order simulated process (Chen and Kareem, 2005).

To obtain $\boldsymbol{\Phi}_n(\omega;\alpha)$ and $\Lambda_n(\omega;\alpha)$ through Eq.(2), the CPSD matrix, $\boldsymbol{S}_F(\omega;\alpha)$, is estimated directly from the wind tunnel realization. In estimating $\boldsymbol{S}_F(\omega;\alpha)$, Welch's method (Welch, 1967) is adopted in this study. The method is based on dividing the signal (e.g., wind load process) into blocks, applying a window (e.g., Hanning window), and averaging their periodograms (Welch, 1967; Solomon Jr, 1991). By averaging a number of periodograms, the noise in the signal is reduced, hence smoothing the spectra and reducing the bias toward a particular realization.

3. Error Assessment

With the aim of quantifying errors associated with using a typical wind tunnel realization to calibrate the stochastic wind model, the target spectra are first defined as the baseline to which spectra obtained from typical wind tunnel realizations as well as simulations can be compared. In this work, the 'target' spectra are obtained from the ensemble average of spectra estimated from many repetitions of the wind tunnel test. The 'typical' spectra are obtained from a single short-duration (e.g., 32 seconds) wind tunnel realization. The 'simulated' spectra are obtained from the simulated process, which was generated following the simulation method of Section 2 where the target spectra were used to calibrate the model.

Three types of errors are investigated that are associated with: (1) typical wind tunnel records, (2) numerical model, and (3) truncation of modes. These errors are assessed based on the second-order statistics of the process, such as the variance and correlation coefficients. In particular, to assess the typical record error, the error of variance, ε_n, is defined here as:

$$\varepsilon_n = \left(\frac{\sigma_n^2 - \sigma_{n_T}^2}{\sigma_{n_T}^2}\right) \times 100\% \tag{4}$$

where σ_n^2 is the variance of the typical realization, estimated through the integration of the 'typical' auto-spectrum, while $\sigma_{n_T}^2$ is the target variance, estimated through the integration of the 'target' auto-spectrum. For the off-diagonal components of the CPSD, the typical record error is estimated in terms of the difference between correlation coefficients, ξ_{np}, as follows:

$$\xi_{np} = \rho_{T,np} - \rho_{R,np} \tag{5}$$

where

$$\rho_{T,np} = \frac{\sigma_{np_T}}{\sqrt{\sigma_{n_T}^2 \sigma_{p_T}^2}} \tag{6}$$

$$\rho_{R,np} = \frac{\sigma_{np}}{\sqrt{\sigma_n^2 \sigma_p^2}} \tag{7}$$

where $\rho_{T,np}$ and $\rho_{R,np}$ are the correlation coefficients of a given pair of components n and p of the 'target' and the 'typical' realization; σ_{np} is the covariance of the typical realization, estimated by integrating the cospectrum (real part of the CPSD); σ_{np_T} is the covariance estimated through the integration of the target cospectrum, where $n = 1, ..., N$, and $p = 1, ..., N$.

It should be noted that a similar scheme to Eqs.(4)-(7) is applied to assess the errors associated with the numerical scheme and mode truncation by replacing the 'typical' realization with the 'simulated' realization considering all modes or a truncated set of modes.

4. Experimentation and Data Processing

Extensive experimental testing was conducted on a rigid rectangular model for multiple wind directions considering a suburban terrain condition. The experiments were carried out at the Natural Hazards Engineering Research Infrastructure (NHERI) Boundary Layer Wind Tunnel (BLWT) at the University of Florida. The pressure acting on the model was simultaneously recorded using a Scanivalve system on a total of 512 pressure taps. The configuration of taps and geometry of the model is shown in Fig. 1(a). The testing was conducted over 15 minutes and repeated five times for multiple wind directions.

The recorded data from the pressure taps were converted to equivalent force coefficients acting on each floor of a 25-story building at a 1:200 scale. The force coefficients are decomposed in the x and y translational directions as well as rotation around the z direction, as shown in Fig. 1(b), and are estimated as:

$$CF_{x,k}(t) = \frac{F_{x,k}(t)}{qB_xH} \tag{8}$$

$$CF_{y,k}(t) = \frac{F_{y,k}(t)}{qB_yH} \tag{9}$$

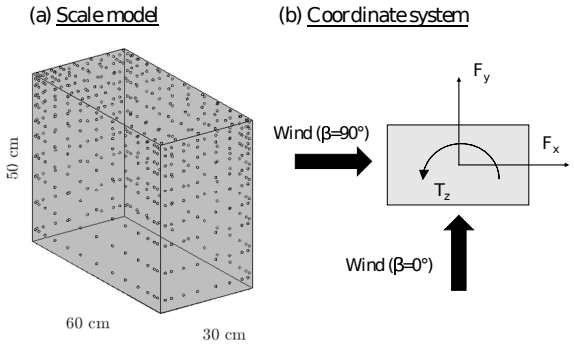

Figure 1: (a) Model geometry and pressure tap configuration; and (b) Coordinate system of forces and wind directions.

$$CT_{z,k}(t) = \frac{T_{z,k}(t)}{qH\frac{B_{\max}^2}{2}} \tag{10}$$

where $CF_{x,k}(t)$, $CF_{y,k}(t)$, $CT_{z,k}(t)$ are the dynamic force coefficients at the kth floor; $F_{x,k}(t)$, $F_{y,k}(t)$, $T_{z,k}(t)$ are the resultant forces and moment estimated from integrating the pressure acting on the tributary area associated with each floor; H is the height of the model; B_x and B_y are the plan dimensions of the building; B_{max} is the maximum plan dimension of the building; q is the dynamic pressure defined as $q = 1/2\rho U_H^2$; ρ is the air density; and U_H is the mean wind speed at the model height. A total of 75 dynamic wind force coefficients are defined for the building, corresponding to the two forces and one moment acting at each of the 25 stories. The dynamic force coefficients were standardized prior to the calibration of the stochastic model to allow a more evenly distributed energy over the eigenvalues, which can enhance the efficacy of mode truncation.

The large wind tunnel dataset was divided into two sets: one set was used to define the target spectra; while the remaining set was used as a testing set to assess errors. Regarding the target spectra for each wind direction, 10 minutes of data from each repetition were used, resulting in a total of 50 minutes of data. This 50-minute dataset was divided into 750 segments of 4-s. The CPSD matrices were estimated and averaged over all 750 segments to obtain the target spectra. As for the testing set, the remaining data were divided into 44 and 45 typical

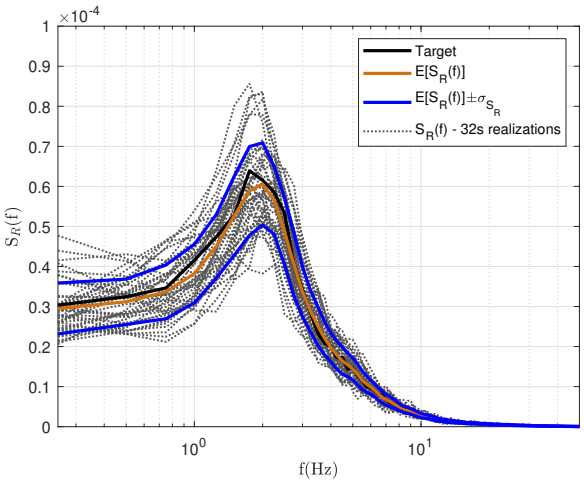

Figure 2: PSD of force coefficient at the 10th floor in the x-direction for $\alpha = 0°$

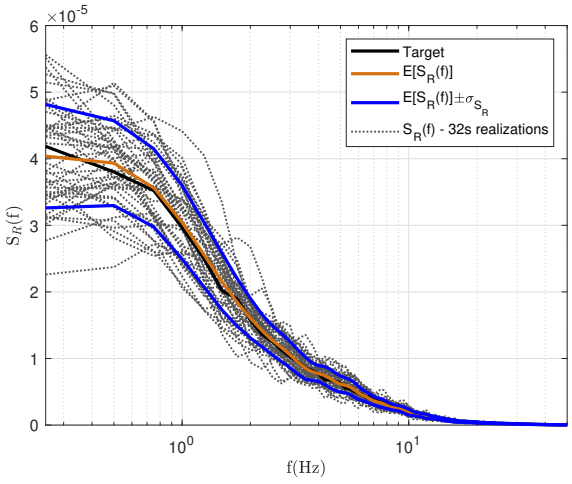

Figure 3: PSD of force coefficient at the 10th floor in the x-direction for $\alpha = 90°$

32-second realizations for $\alpha = 0°$ and $\alpha = 90°$ respectively. Welch's averaging method with a Hanning window and 50% overlap was applied to each realization to obtain the smoothed spectra.

5. Results

5.1. Overview

Three types of errors were assessed using the scheme of Section 4 and are presented in this section for two wind directions, $\alpha = 0°$ and $\alpha = 90°$.

5.2. Typical wind tunnel record error

Figures 2-3 show the smoothed PSD, S_R, for 32-second realizations from the testing data set compared to the target PSD of $CF_x(t)$ at the 10th floor, for $\alpha = 0°$ and $\alpha = 90°$, respectively. It can be observed that the PSDs associated with typical realizations are scattered around the target in both wind directions. This demonstrates that each typical wind tunnel record has some level of variability. Nonetheless, the expected PSD, $E[S_R]$, is close to the target, indicating the consistency of the sampling, therefore allowing the records to be regarded as representative of the stochastic process. For all other components, similar conclusions could be drawn.

For each force component, the mean error of variance, $\mu(\varepsilon)$, was calculated over all typical realizations. Looking over all 75 components, the expectation, $E[\mu(\varepsilon)]$, the maximum, $\max[\mu(\varepsilon)]$, and the minimum, $\min[\mu(\varepsilon)]$, of mean errors were estimated and are summarized in Table 1 for both wind directions. It can be seen that $\mu(\varepsilon)$ varies between $1 \pm 3\%$. This also agrees with the results from Figs. 2-3, at which small biases were observed for $E[S_R]$. The standard deviation, $\sigma(\varepsilon)$, of these errors for each force component was also estimated. The expectation, minimum, and maximum values of $\sigma(\varepsilon)$ over all 75 components are also presented in Table 1. It can be seen that $\sigma(\varepsilon)$ varies between $6 \pm 3\%$, which also confirms the variability observed in Figs. 2-3 for typical records. The error statistics are somewhat close for both wind directions, which may imply that the variability is independent of wind direction.

Similarly, Table 2 presents the expectation, $E[\mu(\xi)]$, minimum value, $\min[\mu(\xi)]$, and maximum value, $\max[\mu(\xi)]$, of the mean errors, $\mu(\xi)$, associated with the correlation coefficients. The results of Table 2 show how $\mu(\xi)$ is contained in the range -0.02 to 0.016, with a certain degree of variability, indicated by the standard deviation, $\sigma(\xi)$, of up to 0.06 – similar behavior as to what was observed for the errors of variance. The error statistics of the correlation coefficients for both wind directions are also close, which may indicate that the variability does not change considerably with wind direction. Other wind directions and experimental settings are currently under investigation.

Table 1: Statistics of the errors in the variance, ε, for $\alpha = 0°$ and $\alpha = 90°$.

α	$0°$	$90°$
$\min[\mu(\varepsilon)]$	-2.49%	-2.66%
$\mathrm{E}[\mu(\varepsilon)]$	-1.28%	0.21%
$\max[\mu(\varepsilon)]$	0.75%	1.81%
$\min[\sigma(\varepsilon)]$	5.84%	4.85%
$\mathrm{E}[\sigma(\varepsilon)]$	7.52%	6.36%
$\max[\sigma(\varepsilon)]$	8.73%	7.25%

Table 2: Statistics of the errors in the correlation coefficients, ξ, for $\alpha = 0°$ and $\alpha = 90°$.

α	$0°$	$90°$
$\min[\mu(\xi)]$	-0.0109	-0.0201
$\mathrm{E}[\mu(\xi)]$	5.8744E-4	0.0011
$\max[\mu(\xi)]$	0.0160	0.0167
$\min[\sigma(\xi)]$	9.56E-17	9.75E-17
$\mathrm{E}[\sigma(\xi)]$	0.0346	0.0350
$\max[\sigma(\xi)]$	0.0566	0.0609

5.3. *Numerical model error*

Figure 4 shows the statistics of the errors associated with the numerical model for various sample sizes ranging between 1,000 and 50,000 simulations for $\alpha = 0°$ and $\alpha = 90°$. For each simulation, a 4-second signal was generated using the target spectra to calibrate the process. A convergence trend is clearly observed when the sample size increases, as is expected in stochastic simulation. The values of $\min[\mu(\varepsilon)]$ and $\max[\mu(\varepsilon)]$ are respectively -0.07% and 0.07% for $\alpha = 0°$, and -0.08% to 0.15% for $\alpha = 90°$ for 50,000 samples. For $\mu(\xi)$, the values range from -2×10^{-3} to 2.6×10^{-3}. This implies the errors introduced by the numerical model are negligible.

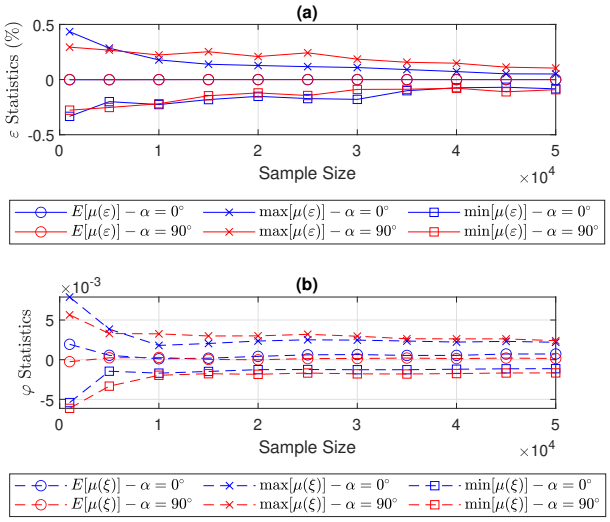

Figure 4: Error associated with the numerical model for different sample sizes, and $\alpha = 0°$ and $\alpha = 90°$: (a) Statistics of ε; and (b) Statistics of ξ.

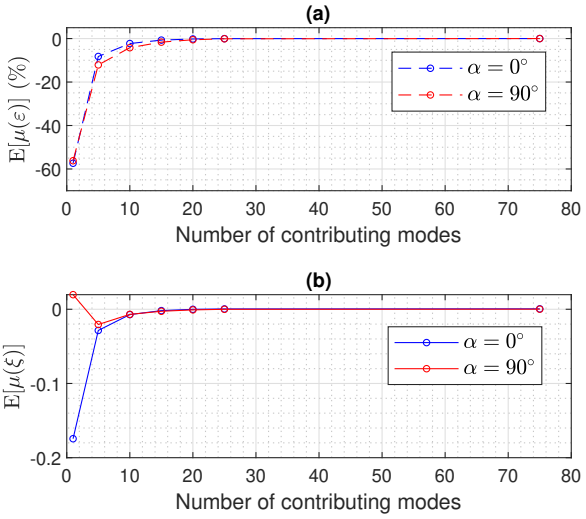

Figure 5: (a) Expected errors of variance, $E[\mu(\varepsilon)]$, for mode truncation; (b) Expected errors of the correlation coefficients, $E[\mu(\xi)]$, for mode truncation.

5.4. *Mode truncation error*

To investigate the errors associated with the truncation of modes, a total of 40,000 samples were generated, considering 1, 5, 10, 15, 20, 25, and 75 modes. The truncation of modes can increase computational speed with minimal effect on the accuracy of the simulation if a sufficient number of modes are considered. Figure 5(a) shows the expected mean error of variance, $E[\mu(\varepsilon)]$, while Fig. 5(b) shows the expected error in the correlation coefficients, $\mathrm{E}[\mu(\xi)]$, for different number of modes. The expected errors clearly decrease as more modes are considered in the simulation. With around 20 modes, 27% of all modes, the errors start to be negligible, on the order of -0.19% to -0.54%. Therefore, even though truncation of modes can be employed in the simulation, the inclusion of higher fre-

quency modes is essential to assure the accuracy of simulation using data-driven POD-based stochastic wind load model.

6. CONCLUSIONS

This study investigated the errors associated with a data-informed POD-based stochastic wind load model for the simulation of stationary multivariate Gaussian processes, such as wind force coefficients. To enable error quantification of the stochastic model, an extensive experimental study on a rigid rectangular model was conducted considering multiple wind directions. In addition to errors associated with the numerical model and mode truncation, errors associated with the use of typical wind tunnel datasets during the calibration of the POD-based stochastic wind load model were investigated. From the preliminary results obtained for the wind directions of 0 and 90 degrees, variability in the spectra calibrated to a typical wind tunnel record was observed and the resulting errors were quantified. Regarding the numerical model, negligible errors are observed. For truncation of modes in the simulation of force coefficients, it is necessary to use a sufficient number of modes to avoid introducing errors in the simulation. However, it is still possible to truncate more than 70% of modes, yet have negligible errors introduced in the simulation. The results provide evidence of the uncertainty associated with the use of typical wind tunnel datasets, as well as guidance on using the wind tunnel-informed stochastic wind load model calibrated to typical wind tunnel datasets. Further analysis for multiple wind directions and the effects when proximity models are included will be conducted subsequently.

7. ACKNOWLEDGEMENTS

The authors would like to gratefully acknowledge the support of the Natural Science Foundation (Grants: CMMI-1750339, CMMI-2131111), and acknowledge Dr. Sungmoon Jung for providing the scale model used in this study.

8. REFERENCES

Arunachalam, S. and Spence, S. M. J. (2022). "Reliability-based collapse assessment of wind-excited steel structures within performance-based wind engineering." *Journal of Structural Engineering*, 148(9), 04022132.

Chen, X. and Kareem, A. (2005). "Proper orthogonal decomposition-based modeling, analysis, and simulation of dynamic wind load effects on structures." *Journal of Engineering Mechanics*, 131(4), 325–339.

Chuang, W.-C. and Spence, S. M. J. (2017). "A performance-based design framework for the integrated collapse and non-collapse assessment of wind excited buildings." *Engineering Structures*, 150, 746–758.

Chuang, W. C. and Spence, S. M. J. (2022). "A framework for the efficient reliability assessment of inelastic wind excited structures at dynamic shakedown." *Journal of Wind Engineering and Industrial Aerodynamics*, 104834.

Davenport, A. (1971). "The response of six building shapes to turbulent wind." *Philosophical Transactions of the Royal Society of London A, Mathematical, Physical and Engineering Sciences*, 269(1199), 385–394.

Deodatis, G. (1996). "Simulation of ergodic multivariate stochastic processes." *Journal of Engineering Mechanics*, 122(8), 778–787.

Kaimal, J. C. and Finnigan, J. J. (1994). *Atmosphoeric boundary layer flows: their structure and measurement*. Oxford University Press.

Ouyang, Z. and Spence, S. M. J. (2020). "A performance-based wind engineering framework for envelope systems of engineered buildings subject to directional wind and rain hazards." *Journal of Structural Engineering*, 146(5), 04020049.

Ouyang, Z. and Spence, S. M. J. (2021a). "A performance-based wind engineering framework for engineered building systems subject to hurricanes." *Frontiers in Built Environment*, 7, 720764.

Ouyang, Z. and Spence, S. M. J. (2021b). "Performance-based wind-induced structural and envelope damage assessment of engineered buildings through nonlinear dynamic analysis." *Journal of Wind Engineering and Industrial Aerodynamics*, 208(1), 104452.

Shinozuka, M. (1971). "Simulation of multivariate and multidimensional random processes." *The Journal of the Acoustical Society of America*, 49(1B), 357–368.

Shinozuka, M. (1987). "Stochastic fields and their digital simulation." *Stochastic Methods in Structural Dynamics*, Springer, 93–133.

Solomon Jr, O. M. (1991). "Psd computations using welch's method.." *Report no.*, Sandia National Labs., Albuquerque, NM (United States), <https://doi.org/10.2172/5688766>.

Suksuwan, A. and Spence, S. M. J. (2018). "Optimization of uncertain structures subject to stochastic wind loads under system-level first excursion constraints: a data-driven approach." *Computers & Structures*, 210, 58–68.

Suksuwan, A. and Spence, S. M. J. (2019). "Performance-based design optimization of uncertain wind excited systems under system-level loss constraints." *Structural Safety*, 80, 13–31.

Welch, P. (1967). "The use of fast fourier transform for the estimation of power spectra: A method based on time averaging over short, modified periodograms." *IEEE Transactions on Audio and Electroacoustics*, 15(2), 70–73.